

Supplemental Material for:
The finite- T Lorentz number and the thermal conductivity.
Aluminum and carbon conductivities from ambient to millions of degrees Kelvin

M.W.C. Dharma-wardana*
National Research Council of Canada, Ottawa, Canada, K1A 0R6,
& Universite de Montreal, Montreal, Canada, H3C 3J7
 (Dated: May 1, 2024)

This supplemental material (SM) covers the following topics:
 (i) Derivation of the finite- T form of the Lorentz number $L_n(t)$
 (ii) Electron-electron interactions in DFT and in conventional approaches.
 (iii) The electrical conductivity from Pseudopotentials and from the T-matrix form of the scattering cross section.
 (iv) Results for l -Al at 2.7 g/cm³, l -carbon at 10 g/cm³, and at the “diamond-like” density of 3.6 g/cm³.

PACS numbers: 52.25.Jm, 52.70.La, 71.15.Mb, 52.27.Gr

I. DERIVATION OF THE FINITE- T FORM OF THE LORENTZ NUMBER

We use Hartree atomic units, with $\hbar = m_e = |e| = 1$, and T such that the Boltzmann constant $k_B = 1$. The symbols defined in the main text are also used in this supplemental material without further definition unless additional clarification is needed.

In the following we use the following normalization of the Fermi function:

$$\bar{n} = \int \frac{d\vec{k}}{4\pi^3} f(k) \quad (1)$$

$$f(k) = f(\epsilon) = 1/[1 + \exp(\epsilon - \mu)/T] \quad (2)$$

$$\epsilon = k^2/2. \quad (3)$$

Then the classical limit is given by

$$f(\epsilon) = \exp(\mu/T) \exp(-\epsilon/T) \quad (4)$$

$$e^{(\mu/T)} = \frac{\bar{n}}{2} \left[\frac{2\pi}{T} \right]^{3/2}. \quad (5)$$

The above normalization is commonly used [1], but differs from the usage in some standard texts [2]. Furthermore, in the NPA, the volume occupied by the free electrons is *not* the ionic Wigner-Seitz sphere of radius $r_{ws} = \{3/4\pi\bar{\rho}\}^{1/3}$, but an infinitely large volume, approximated by a volume of radius R_c of the “correlation sphere” of the fluid. It is such that, given a nucleus placed at the origin of the correlation sphere, all pair-distribution functions $g_{ss'}(r)$, where the species s or s' may be electrons or ions, have decayed to unity when $r \rightarrow R_c$. For $T < E_F$, usually $R_c \sim 10r_{ws}$, while for higher T we have used $R_c \sim 5r_{ws}$.

The non-interacting electrons (i.e., Kohn-Sham electrons) populating the correlation sphere take the non-interacting value μ^0 for its chemical potential, as required by DFT. This model is discussed in more detail in Refs. [3, 4]. Average-atom models that confine the free electrons to within the ionic Wigner-Seitz sphere become similar to our NPA model for T sufficiently large, such that $g_{ie}(r) = n(r)/\bar{n}$ has already decayed to unity as $r \rightarrow r_{ws}$.

We define the kinetic coefficients \mathcal{L}^α as in Ashcroft and Mermin, Chapter 13 [1]. We use the notation $\langle \dots \rangle$ used in the main text to indicate averaging over $-df(\epsilon)/d\epsilon$. Then,

$$\mathcal{L}^\alpha = \langle (\epsilon - \mu)^\alpha \tau(\epsilon) I(\epsilon) \rangle \quad (6)$$

$$I(\epsilon) = \int \frac{d\vec{k}}{4\pi^3} \delta(\epsilon - \epsilon(\vec{k})) \vec{V}_{\vec{k}} \vec{V}_{\vec{k}}. \quad (7)$$

As we are considering a uniform fluid with $\epsilon(\vec{k}) = k^2/2$, $\vec{V}\vec{V} = (1/3)V^2$, the above equation can be written as:

$$\mathcal{L}^\alpha = C_0 \langle (\epsilon - \mu)^\alpha \epsilon^{3/2} \tau_{ei}(\epsilon) \rangle \quad (8)$$

$$C_0 = \frac{2\sqrt{2}}{3\pi^2} \quad (9)$$

A generic form for $\tau_{ei}(\epsilon)$ can be obtained from the Rutherford formula for the scattering of an electron by a heavy ion of charge \bar{Z} . This leads to the Landau-Spitzer form if written in terms of a Coulomb Logarithm C_{lg} (see Sec 44, of [2]). Here we have restored the constants m_e and e for clarity.

$$\tau_{ei}(\epsilon) = \frac{m_e^{1/2} (2\epsilon)^{3/2}}{4\pi Z e^4 \bar{n} C_{lg}} \quad (10)$$

$$= C_{ei} \epsilon^{3/2} \quad (11)$$

A more sophisticated calculation of the scattering, inclusive of the ion-distribution by including a structure factor, pseudopotentials or a T-matrix usually amounts

* Email address: chandre.dharma-wardana@nrc-cnrc.gc.ca

to an improved form for C_{lg} . Our main purpose here is to provide a tractable form for $\tau_{ei}(\epsilon)$ to evaluate the kinetic coefficients analytically, and the analysis remains valid as long as any improved form for C_{lg} does not introduce any additional dependence on ϵ . Then, for $T > 0$, the $df/d\epsilon$ can be reduced by a partial integration to give:

$$\mathcal{L}^{(0)} = C_1 \int d\epsilon f(\epsilon) 3\epsilon^2, \quad C_1 = C_0 C_{ei} \quad (12)$$

$$\mathcal{L}^{(1)} = C_1 \int d\epsilon f(\epsilon) (4\epsilon^3 - 3\mu\epsilon^2) \quad (13)$$

$$\mathcal{L}^{(2)} = C_1 \int d\epsilon f(\epsilon) (5\epsilon^4 - 8\mu\epsilon^3 + 3\mu^2\epsilon^2) \quad (14)$$

These results can be incorporated into the expression for the Lorentz number L_N .

$$L_N = \frac{1}{T^2} \left[\frac{\mathcal{L}^{(2)}}{\mathcal{L}^{(0)}} - \left(\frac{\mathcal{L}^{(1)}}{\mathcal{L}^{(0)}} \right)^2 \right] \quad (15)$$

$$= \frac{5I_4(\eta)}{3I_2(\eta)} - \left(\frac{4I_3(\eta)}{3I_2(\eta)} \right)^2 \quad (16)$$

$$I_n(\eta) = \int_0^\infty dx \frac{x^n}{1 + \exp(x - \eta)}, \quad \eta = \mu/T \quad (17)$$

Thus $L_N = L_N(\eta)$ is dependent only on $t = T/E_F$ since η , the reduced chemical potential depends only on t . Furthermore, in a DFT-implementation, μ is the *non-interacting* chemical potential μ^0 of Kohn-Sham electrons.

The reduction of \mathcal{L}^α given above is not applicable in the limit $T = 0$ when $df/d\epsilon$ reduces to a delta-function. Then the kinetic coefficients containing any $(\epsilon - \mu)$ factors reduce to zero. Consequently a Sommerfeld expansion about $\epsilon = E_F$ is needed. In the limit $T \rightarrow 0$ it can be shown that:

$$\kappa = (1/3)C_e \langle V^2 \rangle \tau_{ie}, \quad t \sim 0 \quad (18)$$

Here C_e is the electron specific heat per particle, while $\langle V^2 \rangle$ is an electron mean square-velocity evaluated within the thermally smeared scattering region $E_F \pm T$ in k -space enclosing the Fermi energy. We take this to be

$$\langle v^2 \rangle = \langle V^2 \rangle / \langle 1 \rangle \quad (19)$$

$$= 6T \frac{I_{1/2}(\eta)}{I_{-1/2}(\eta)} \quad (20)$$

The electron specific heat is approximated from the temperature derivative of the total internal energy $E_e = E_0 + E_{xc}$ of the uniform electron fluid (UEF) at the r_s and T corresponding to the \bar{Z} of the material studied. Thus, for l -Al at 2.35g/cm³ at the melting point ~ 933 K, $\bar{Z} = 3$ and $r_s = 2.171$, the case studied by Recoules et al [5]. However, we study Al at 2.7 g/cm³, $r_s = 2.07322$.

The ideal UEF energy E_0 and C_e^0 are easily calculated, while E_{xc} is available from several analytic models [6,

7], as well as empirically from numerical simulations [8]. The simulation data have been parametrized for the free energy $F(r_s, t)$ [9, 10]. The second T -derivative of the parametrized $F(r_s, t)$ is needed for C_e . Consequently, artifacts of the parametrization may affect the calculated C_e [11].

However, Eq. 18 is applicable only essentially at $T = 0$ and the problems with the finite- T XC-parametrization arise only for t well beyond the regime of validity of Eq. 18. The only result that we use from Eq. 18 is the limiting value of L_N at $T = 0$ that is used in the fit function that extends the domain of Eq. 15 to $T = 0$ as well.

The approach used here can also be used to obtain the thermoelectric coefficient as well. However, we will not present calculations of these other transport coefficients. Furthermore, the electron XC-effects, embedding-energy effects etc., neglected here would be treated in a separate study.

II. TRANSPORT COEFFICIENTS AND ELECTRON-ELECTRON INTERACTIONS

The total Hamiltonian of a system of electrons and ions that we consider can be written in a self-evident notation as:

$$H = \sum_s H_0^s + H_{ii} + H_{ei} + H_{ee}, \quad (21)$$

The ideal terms H_0^s , $s = i, e$ contain the kinetic energy of non-interacting particles of type s . In the type of systems that we consider in this study, the electric current and the heat current are carried by the electrons, as the ions are treated mainly as heavy scattering centers that provide resistance to electron flow under the applied gradients of temperature or electric potential. If we consider the calculation of the electrical conductivity, this can be done via the Boltzmann equation, or via the current-current correlation function of Kubo theory.

While the scattering of electrons from heavy, essentially static ions is easily addressed by these theoretical methods, the effect of scattering of electrons, and how they affect the electrical conductivity (and other transport coefficients) are more complex. The collision frequencies ν_{ei} and ν_{ee} are assumed separable and are usually evaluated independently in such treatments. Systems where ν_{ee} are neglected are referred to as ‘‘Lorentz plasmas’’. Here we argue that DFT provides a means of side-stepping this problem by mapping any election-ion plasma to an equivalent Lorentz plasma. The two-body e-e interaction, H_{ee} , is replaced by a one-body XC-correlation functional.

Usually the electron distribution function $f(k)$ perturbed by the electric field to $f(k) = f_0(k) + \delta f(k)$ is considered. Here $\delta f(k)$ is small and linear in the applied (very weak) field. The effect of H_{ee} enters into transport coefficients via the modification of the screening function

(e.g., from the Lindhard function to RPA and beyond) contained in the scattering cross section, and by its effect on $\delta f(k)$. The heat current is additionally modified by the effect of e-e interactions on the electron specific heat. These quantities are evaluated to some order in perturbation theory by traditional treatments of distribution functions, quantum Green's functions, diagrammatic methods etc., in dealing with H_{ee} .

The difficulties and uncertainties inherent in this process may be understood by examining the inclusion of e-e interactions in the dielectric function, or equivalently, in the response function $\chi(k, \omega)$ of the uniform electron fluid at finite- T , or even at $T = 0$. A treatment using the two-temperature Zubarev Green's functions has been given by the present author [12]. A major problem in these approaches is to obtain a conserving approximation, in the sense that the Ward identities, Gauge invariance etc., should be obeyed by the approximation. Richardson and Ashcroft [13] provided such a finite- T calculation to second order in the screened interaction. Applying the technique to the case of partially degenerate hydrogen plasma [14] leads to results which are extremely difficult to compute. It is difficult to ascertain if existing quantum-kinetic results for e-e corrections to transport coefficients are conserving approximations.

The advent of density functional theory has provided an elegant solution to this problem. DFT shows that the two-body H_{ee} may be replaced by a one-body XC-functional where the interacting electron gas is mapped to an equivalent non-interacting electron system at the interacting-fluid density.

$$H = (H_0^i + V_{xc}^i([\rho])) + (H_0^e + V_{xc}^e([n]) + H_{ei}) \quad (22)$$

Here the two-body ion-ion interaction has been replaced an ion-XC potential [3]. It is this $V_{xc}^i([\rho])$ that enables us to use one-ion DFT, viz., the NPA, instead of the N -ion DFT used in QMD. The two-body e-e interaction is replaced by an electron-XC potential $V_{xc}^e([n])$ for which many finite- T parametrizations are available. In Eq. 22 the original Hamiltonian is reduced to that of a Lorentz plasma with no two-body e-e scattering. Thus, if transport coefficients are calculated using DFT-generated cross sections, distribution functions etc., then no ν_{ee} contributions need to be included, although such corrections may be needed in non-DFT theories of Spitzer and Härrm [15], Reinholtz et al [16] and others.

In our NPA calculations, the scattering cross section is expressed either in terms of a screened pseudopotential $U_{ei}(k)/\varepsilon(k)$, or via a T-matrix. The pseudopotential is $u_{ei}(k) = \Delta n_f(k)/\chi(k)$, where $\chi(k)$ is the electron response function. It is for an ion with an effective charge $\bar{Z} = n_f$ and a rigid core of bound electrons with n_b electrons. The nuclear charge of the ion $Z_n = n_b + n_f$. The electron XC functional enters into the determination of $n_f(r)$ and hence into all the distribution functions.

Similarly, the T-matrix provides a scattering cross section which involves the phase shifts that result from interactions with the nucleus as well as all the electrons,

bound and free, via the electron XC potential as well as the Coulomb interactions. The collision frequency ν_{ei} calculated via either the NPA $U_{ei}(k)$, or via the NPA generated T-matrix is for Kohn-Sham electrons constituting a Lorentz plasma which *already incorporates the e-e collisions* in a non-factorizable way, and to all orders in the e-e interaction.

III. THE ELECTRICAL CONDUCTIVITIES FROM THE T-MATRIX AND FROM $U_{ei}(k)$

In Fig. 1 we have displayed a number of calculations of the isochoric conductivity of l -aluminum at 2.7 g/cm³.

As first noted by Perrot and the present author in 1999 [19], these results confirm that σ_z from pseudopotential-based calculations, and σ_{tmx} from T-matrix based calculations, differ significantly. The differences appear when Al³⁺ begins to loose core electrons, with \bar{Z} increasing beyond three. The Al³⁺ ion has a robust filled core with the electronic configuration: $1s^2 2s^2 3p^6$. An electron moving under an applied field will scatter from it elastically, with no interaction with the core except for a form factor already included in the weak pseudopotential. Interactions between continuum electrons and core electrons are possible but these are not elastic collisions (where the energy change $\omega \neq 0$).

$$U_{ei}(k) = \Delta n_f(k)/\chi(k) \quad (23)$$

$$\chi(k) = \chi^0(k)/[1 + v_k(1 - G_k)\chi^0(k)] \quad (24)$$

Here $v_k = 4\pi/k^2$, and $\chi^0(k)$ is the Lindhard function for non-interacting electrons. The local-field correction G_k contains XC-corrections. The use of the pseudopotential corresponds to the use of the Hamiltonian

$$H = H_0 + \sum_{\vec{k}, \vec{k}_1, \vec{k}_2} U_{ei}(k) A_{\vec{k}_1}^\dagger a_{(\vec{k}_2 + \vec{k})}^\dagger a_{\vec{k}_2} A_{(\vec{k}_1 + \vec{k})} + \text{other terms} \quad (25)$$

Here $A_{\vec{k}}^\dagger, A_{\vec{k}}$ are creation and annihilation operators for ions, while $a_{\vec{k}}^\dagger, a_{\vec{k}}$ are for electrons. The matrix elements are written to indicate momentum conservation to be formally exact, but this is irrelevant for massive ions usually treated in the Lorentz plasma model; the momenta of ion-density fluctuations $\rho_k^\dagger = \sum_{\vec{k}_1} A_{\vec{k}_1 + \vec{k}}^\dagger A_{\vec{k}_1}$ are not conserved unless ion dynamics is included.

If the ion core is robust, and if $U_{ei}(k)$ is weak, as is the case for Al³⁺, multiple scattering effects, strong-collisions etc., are negligible and the T-matrix results should agree with those from the weak pseudopotential. Numerical limitations in our codes prevent us from extending the T-matrix calculation of the conductivity to low temperatures to verify this explicitly. In fact, our σ_{tmx} for Al becomes increasingly inaccurate for $T < 3$ eV. In fig. 1 we have joined the σ_z with σ_{tmx} with a straight line to indicate the transition region where the pseudopotential model begins to breakdown, while the T-matrix method

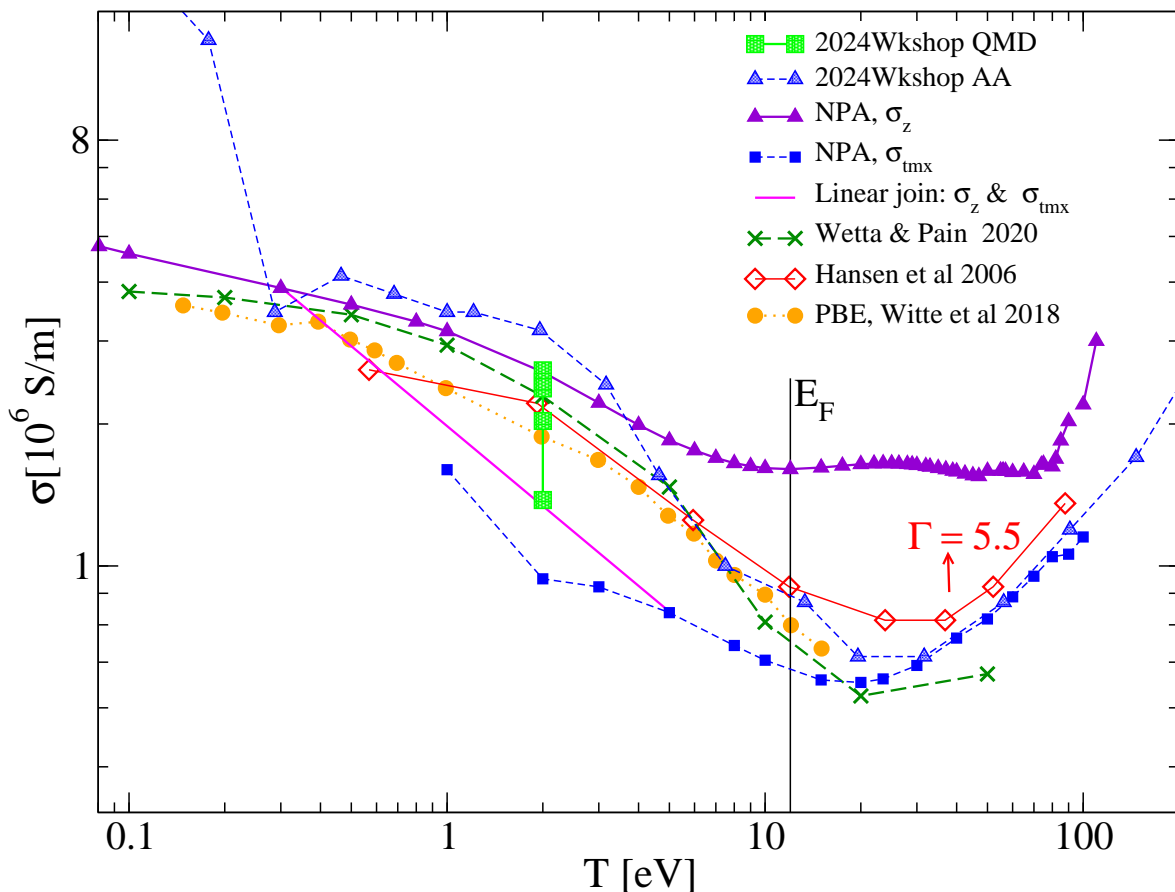


FIG. 1. (Color online) The isochoric conductivities σ_z, σ_{tmx} calculated via the Ziman formula with NPA inputs, for l -aluminum, are compared with representative AA, QMD and other results. Results given in Ref. [17] are labeled “2024 Wkshop”. The five QMD results at 2 eV use several different XC-functionals. Witte et al, 2018 [18] refers to QMD calculations using the $T = 0$ Perdew-Burke-Ernzerhof XC-functional. Wetta & Pain 2020 [23]; Hansen et al 2016 [24]. The value of E_F displayed corresponds to $\bar{Z} \sim 3$, but this increases as T increases, as seen in Table III.

becomes appropriate. In this region core states acquire partial occupancies while $\bar{Z} > 3$ has a fractional value and an integer part.

The partial occupancies in the core provide a mechanism for some of the conduction electrons to become “hopping electrons” [20], and the value of the conductivity depends on how these electrons are treated in the conductivity model. Partial occupancies of core states make it possible for continuum electrons to interact with core electrons while the overall energy is conserved, as in elastic collisions, while the momentum need not be conserved as the ions are assumed to be infinitely heavy. For instance, an electron in a k, l state of energy $k^2/2$ may fall into a partially occupied $3p$ state while an electron in such a $3p$ may be ejected to a k, l' state of energy $k^2/2$. That is, the T-matrix approach includes additional scattering channels that are not included in the ion with a rigid-core implied by the pseudopotential $U_{ei}(k)$.

The phase shifts that are used to construct the T-matrix are such that:

(i) they satisfy the finite- T Friedel sum rule [3] that sets

the value of \bar{Z} self-consistently with the ionization balance and thermodynamics;

(ii) they provide a consistent treatment of strong collisions that takes account of the partially ionized states of the core and any continuum resonances.

Given that the numerical results of the pseudopotential model differ very significantly from the strong-collisions model already at, say, $T = 2$ eV, one would wonder why the pseudopotential model is successful in accurately predicting the pair-distribution functions of l -Al at 1 eV, or 2 eV, etc., in the sense that the $g(r), S(k)$ obtained from the NPA pair-potentials agree very well from QMD calculations. The agreement of NPA pair-distribution functions with those of QMD has been demonstrated in many previous publications (e.g., [21, 22]). The reason for this is that the ion-ion pair potential involves a strong repulsive term $\bar{Z}^2 V_k$, which is not there in the electron-ion interaction. The latter is essentially an attractive interaction that encourages close collisions; furthermore, any Pauli blocking that exists in fully occupied core states is removed for partial occupancies.

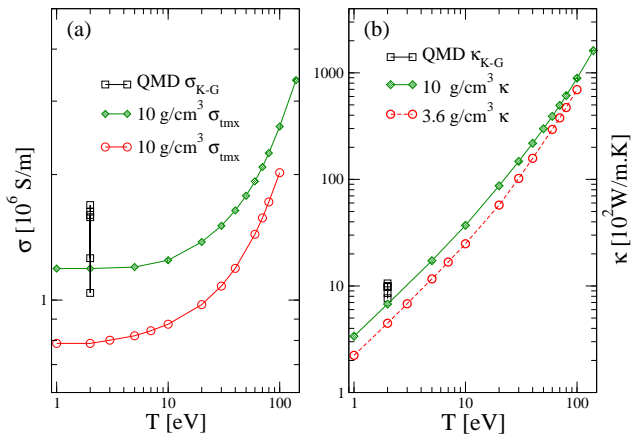


FIG. 2. (Color online) (a) The isochoric conductivities σ_{tmx} for l -carbon at 10 g/cm^3 and 3.6 g/cm^3 from NPA calculations. (b) The corresponding NPA- κ obtained via the Lorentz number $L_N(t)$. The QMD results for σ and κ for l -C at 10 g/cm^3 , $T=2 \text{ eV}$ reported in Ref. [17] are also displayed.

These same issues affect the accuracy of the Kubo-Greenwood approach in calculating a $\sigma(\omega)$ and extrapolating to $\omega \rightarrow 0$ via some rigid-core model, e.g., the Drude model. The sensitivity of σ_{K-G} obtained from QMD to the XC-functionals emphasizes this difficulty. In Fig. 1, the QMD K-G σ for Al at 2.7 g/cm^3 takes the highest value of $2.6 \times 10^6 \text{ S/m}$ for a calculation using the PBE functional, while the lowest value is nearly half, viz., $1.38 \times 10^6 \text{ S/m}$ is for the SCAN functional. It should be noted that as the number N of ions used in a QMD simulation increases, the complex character of possible ionic configurations of “bonding schemes” increases, and the corresponding electron distributions become very complex, demanding more and more complex XC-functionals. In contrast, in the NPA and in AA models there is only one ion and the corresponding electron density is a simple smooth density with the main rapid changes and discontinuity being at the nucleus. Consequently, NPA calculations are insensitive to the XC-functional used.

Furthermore, since QMD implementations do not usually incorporate finite- T XC-functionals, the corrections to the specific heat from XC-effects are not included in such calculations, thus affecting the calculation of κ .

IV. TABULATED DATA FOR ALUMINUM AND CARBON

In this section we provide some representative results for isochoric σ and κ for l -carbon, and l -aluminum at 2.70 g/cm^3 . The l -carbon data are at the density 10.0 g/cm^3 and at the “diamond-like” density of 3.6 g/cm^3 . The σ_{tmx} is calculated using the NPA, and κ is obtained

from the numerical fit to the Lorentz number $L_N(t)$.

A sample of tabulated results for l -carbon at 10 g/cm^3 is give in table I

At low temperatures, the resistivity “saturates” as the

TABLE I. The isobaric conductivity σ_{tmx} , and κ for l -C at 10 g/cm^3 . The thermal conductivity is calculated from σ using the finite- T Lorentz number $L_N(t)$ defined in the main text. More digits than warranted by physical accuracy are shown for technical reasons (e.g., useful in identifying the version of a code used to generate the results).

Tev	σ_{tmx}	\bar{Z}	$\kappa/10^2$
1	1.190	4.000	3.373
2	1.190	4.000	6.743
5	1.191	4.000	16.89
10	1.246	4.000	35.34
20	1.378	4.000	78.40
40	1.640	4.003	193.4
60	1.927	4.042	365.2
80	2.252	4.158	595.4
100	2.608	4.337	879.6
140	3.369	4.733	1613

l -carbon structure factor adjusts to have a maximum at $2k_F$ as $T/E_F \rightarrow 0$, when electron-ion scattering is maximized as in Friedel-controlled fluids [22]. We see essentially the same behaviour in carbon at the “diamond-like” density of 3.6 g/cm^3 , (see Table II). The data for l -carbon at these two densities are displayed in Fig. 2.

TABLE II. The isobaric conductivity σ_{tmx} , and κ for l -C at 3.6 g/cm^3 . The thermal conductivity is calculated from σ using the finite- T Lorentz number $L_N(t)$ defined in the main text.

Tev	σ_{tmx}	\bar{Z}	$\kappa/10^2$
1.0	0.787	4.000	2.233
2.0	0.787	4.000	4.464
3.0	0.801	4.000	6.813
5.0	0.821	4.000	11.64
10.0	0.875	4.000	24.89
20.0	0.975	4.000	57.41
40.0	1.191	4.005	157.6
60.0	1.438	4.073	294.5
80.0	1.719	4.267	472.4
100.0	2.021	4.530	695.5

[1] N. W. Ashcroft and N. D. Mermin, Solid State Physics, Ch. 13. Saunders College, Philadelphia, USA (1976).

[2] E. M. Lifshitz and L. P. Pitaevskii, *Physical Kinetics*,

TABLE III. The isobaric conductivity σ_{tmx} (σ_z if in parenthesis), and κ for l -Al at 2.7 g/cm^3 . The thermal conductivity is calculated from σ using the finite- T Lorentz number $L_N(t)$ defined in the main text. More digits than warranted by physical accuracy are shown for technical reasons (e.g., useful in identifying the version of a code used to generate the results).

Tev	σ_{tmx}	\bar{Z}	$\kappa/10^2$
0.1	(4.60)	3.000	1.303
0.3	(3.89)	3.000	3.309
5	0.796	3.000	12.83
8	0.678	3.003	15.98
10	0.631	3.016	21.19
20	0.566	3.495	38.62
30	0.615	4.299	63.22
40	0.703	5.085	96.55
60	0.860	6.233	177.5
80	1.046	7.296	288.2
100	1.152	7.720	396.9

Pergamon, New York (1981).

- [3] M. W. C. Dharma-wardana and F. Perrot, Phys. Rev. A **26**, 2096 (1982).
- [4] F. Perrot and M.W.C. Dharma-wardana, Phys. Rev. E. **52**, 5352 (1995).
- [5] V. Recoules and J. P. Crocombette, Phys. Rev. B **72**, 104202 (2005).
- [6] F. Perrot and M. W. C. Dharma-wardana, Phys. Rev. B **62**, 16536 (2000); *Erratum*: **67**, 79901 (2003); arXiv-1602.04734.
- [7] F. Perrot and M. W. C. Dharma-wardana, Phys. Rev. A **30**, 2619 (1984).
- [8] Ethan W. Brown, J. L. Dubois, J. L. Dubois, Markus Holzmann, David Ceperley Phys. Rev B **88**, 081102(R) (2013).
- [9] V. V. Karasiev, T. Sjoström, J. W. Dufty, and S. B. Trickey, Phys. Rev. Lett. **112**, 076403 (2014).
- [10] Tobias Dornheim, Simon Groth, Michael Bonitz Physics Reports, **744**, 1-86 (2018), <https://doi.org/10.1016/j.physrep.2018.04.001>.
- [11] V. Karasiev, S. B. Trickey and J. W. Dufty. Phys. Rev. B **99**, 195134 (2019).
- [12] M. W. C. Dharma-wardana J. Phys. C. **9**, 1919 (1976).
- [13] C. F. Richardson and N. W. Ashcroft, Phys. Rev. B **50**, 8170 (1994).
- [14] M. W. C. Dharma-wardana, Physica, **92A**, 59-86 (1978).
- [15] L. Spitzer and R. Härm, Phys. Rev. **89**, 977 (1953).
- [16] H. Reinholz, G. Röpke, S. Rosmej, and R. Redmer, Phys. Rev. E **91**, 043105 (2015).
- [17] L. J. Stanek, A. Kononov, S. B. Hansen, et al. *Review of the Second Charged-Particle Transport Coefficient Code-Comparison Workshop*. Unpublished (2023).
- [18] B. B. L. Witte, P. Sperling, M. French, V. Recoules, S. H. Glenzer, and R. Redmer, Physics of Plasmas **25**, 056901 (2018).
- [19] F. Perrot and M. W. C. Dharma-wardana, Int. J. of Thermophys, **20**, 1299 (1999).
- [20] M.W.C. Dharma-wardana and F. Perrot, Phys. Rev. A **45**, 5883 (1992).
- [21] L Harbour, and G. D. Förster, M. W. C. Dharma-wardana and Laurent J. Lewis, Physical review E **97**, 043210 (2018).
- [22] M. W. C. Dharma-wardana, Lucas J. Stanek, and Michael S. Murillo Phys. Rev. E **106**, 065208 (2022).
- [23] N. Wetta and J.-C. Pain, Phys. Rev. E **102**, 053209 (2020).
- [24] S. B. Hansen, W. A. Isaacs, P. A. Sterne, B. G. Wilson, V. Sonnad, D. A. Young Proceedings of the NEDPC2005; Technical Report: UCRL-PROC-218150 Lawrence Livermore (US) National laboratory, Livermore, USA (2006).

The finite- T Lorentz number and the thermal conductivity. Aluminum and carbon conductivities from ambient to millions of degrees Kelvin

M.W.C. Dharma-wardana*

National Research Council of Canada, Ottawa, Canada, K1A 0R6,
§ Université de Montreal, Montreal, Canada, H3C 3J7

(Dated: May 1, 2024)

Theoretical prediction of the thermal conductivity κ of metal-like electron-ion systems would be greatly simplified if a convenient generalization of the Lorentz number L_N for arbitrary temperatures (T) and densities were available. Such calculations are needed in astrophysics, high-energy-density physics, semiconductor physics as well as in materials science. We present a finite- T form of $L_N(T)$, expressed in terms of elementary Fermi integrals. It is a universal function of $t = T/E_F$, where E_F is the Fermi energy of the electrons. A convenient four-parameter fit to $L_N(t)$ for $t = 0 - \infty$ further simplifies the applications. The effect of electron-electron interactions is also briefly discussed. Calculations for $L_N(t)$ and thermal conductivities κ for Al and C are presented at several compressions and into the million-Kelvin range. Experimental isobaric conductivities for Al just above the melting point, and isochoric conductivities for Al and C from available density-functional theory simulations and average-atom calculations are used as comparisons.

PACS numbers: 52.25.Jm, 52.70.La, 71.15.Mb, 52.27.Gr

Introduction- Modern studies in materials science, be it for hydrogen storage or astrophysical and warm dense matter (WDM) applications, seek to predict the relevant target physical properties prior to costly and time-consuming experimentation. In many cases of WDM, and most astrophysical systems, experimentation is usually impossible except for narrow ranges of the phase diagram. These systems straddle intermediate regimes of matter extending from cold solids to hot plasmas, at various densities and states of ionization [1–3, 5–9]. The same issues arise in high-energy-density applications where energy is deposited in femto-second time-scales producing multi-temperature quasi-equilibria [9–13] where temperature-relaxation rates are of interest. The electrons and holes in semi-conductor nanostructures also behave like WDM systems due to the small effective masses of the charge carriers [14].

While crystalline solids are defined by a few atoms in a unit cell, systems above the melting point pose challenges for traditional N -atom density-functional theory (DFT) and molecular-dynamics (MD) based simulations where N must be made as large as possible. The ions are usually modeled as classical particles, where as the electrons are treated quantum mechanically [15]. If finite temperatures are to be treated, then the number of basis functions needed for the quantum calculation becomes prohibitively high, when the temperature T (in energy units) exceeds the Fermi energy E_F . This N -atom DFT-MD approach will be referred to as the quantum molecular dynamics (QMD) method. Its current implementations do not usually include finite- T electron exchange and correlation (XC) effects although finite- T functionals are available [16–21]. In QMD, N -ions are explicitly simulated while the electron-electron interaction is reduced

to a one-electron problem.

Instead of QMD we use the neutral-pseudo-atom model (NPA), a rigorous DFT approach [3, 4] that eliminates explicit simulation of N -ions by invoking an ion-ion XC functional (in addition to the e-e XC functional), to incorporate multi-ion effects. In the NPA, the free-electron density $n_f(r)$ and the mean free-electron density \bar{n} are available from the Kohn-Sham calculation for a single nucleus immersed in the fluid defined by its self-consistently determined one-body densities $n(r)$ and $\rho(r)$ for electrons and ions respectively. The density increment $\Delta n_f(k) = n_f(k) - \bar{n}$ serves to define a weak pseudopotential $U_{ei}(k)$ that may be used in evaluating the ion-ion $S(k)$, and in transport calculations (static fields). The pseudopotential subsumes the internal structure of the ion and describes a rigid scatterer. The T-matrix constructed from the phase-shifts of the NPA calculation can also be used in the Ziman-Evens formula and can be sensitive to the internal structure of the ion.

Calculations of *static* transport quantities in QMD are complex, indirect and mired in many assumptions. In QMD, Kohn-Sham electronic states and energies are generated for a succession of *fixed* configurations of N -ions used in the simulation, thus neglecting ion-dynamical effects and coupled-mode effects that are important near low-frequencies $\omega \rightarrow 0$. Typically $64 \leq N \leq 512$. The dynamic conductivity of the fluid, $\sigma(\omega)$, is evaluated as a thermal average of the crystalline $\sigma_c(\omega)$ values of ‘all’ periodic solids constructed from the N -ions in the QMD simulation. The Kubo-Greenwood (KG) formula [22, 23] is used for $\sigma(\omega)$. The local-field corrections arising from the crystalline band structure [24] are ignored, and the calculated KG- $\sigma(\omega)$, lacking in ion dynamics diverges as $\omega \rightarrow 0$. Hence at this stage a Drude model or other model [25, 26] that assumes a rigid internal structure for the ions, and a scattering potential that remains unchanged over the long-time scales of the $\omega \rightarrow 0$ collisional

* Email address: chandre.dharma-wardana@nrc-cnrc.gc.ca

limit are assumed to extrapolate $\sigma(\omega)$ to $\sigma(0)$. The evaluation of κ proceeds via the kinetic coefficients of semi-classical transport theory [23, 27].

The Lorentz number L_N is traditionally evaluated from independently determined σ and κ . The temperature T_k is usually expressed in Kelvin.

$$L_N(T_k) = \frac{\kappa}{\sigma(0)T_k} = \frac{\kappa}{\sigma T} \left[\frac{k_B}{e} \right]^2. \quad (1)$$

We use Hartree atomic units, with $\hbar = m_e = |e| = 1$, and T such that the Boltzmann constant $k_B = 1$. The electron Wigner-Seitz radius r_s is given by $r_s = (3/4\pi\bar{n})^{1/3}$. The number of free electrons per ion, viz., \bar{Z} is $\bar{n}/\bar{\rho}$, where $\bar{\rho}$ is the mean ion density.

The Lorentz number of ideal electrons scattering from a system of heavy ions (Lorentz gas) at $T = 0$, and for $T \rightarrow \infty$ (classical limit) is well known. Here we derive a result for arbitrary degeneracies and densities in terms of elementary Fermi integrals. Then $L_N(T, r_s)$ is found to be a universal function of $t = T/E_F$ only, where E_F is the Fermi energy. Hence, given an estimate of σ , the thermal conductivity κ is immediately known via $L_N(t)$. At this stage electron-electron interactions and ion-embedding effects are neglected.

Electron-electron interactions are included in traditional transport theories by additional corrections via the Boltzmann equation [28], via perturbation corrections to kinetic equations and distribution functions etc [29–31]. However, if phase-shifted plane waves are eigenstates of electrons, no contributions from e-e interactions arise. Constructing higher-order theories to include e-e interactions within conserving approximations is very difficult, especially at finite- T [32]. DFT solves the problem of e-e interactions by mapping interacting electrons to non-interacting Kohn-Sham electrons experiencing just a one-body XC-potential. Hence no further e-e corrections are needed if NPA generated $U_{ei}(k)$, $S(k)$, T-matrices etc., are used in transport calculations (see SM [33]) as they already include finite- T XC effects.

Explicit isochoric calculations for liquid Al (l -Al) at $\bar{\rho}=2.7$ g/cm³, 2.35 g/cm³ are presented, while isobaric calculations are presented for the densities studied experimentally by Leitner et al [34]. Calculations of the Lorentz number, electrical and thermal conductivities for l -C at $\bar{\rho}=10$ g/cm³ and at the diamond-like density of 3.6 g/cm³ (see SM) are also presented and compared with any available published data.

The Lorentz number and the conductivities- In the semi-classical theory of transport, the kinetic coefficients $\mathcal{L}^{(\alpha)}$ are used to express the conductivities. Their detailed definitions and reduction to simple forms within a Lorentz-plasma model are given in SM [33]. Then we have

$$\sigma = \mathcal{L}(0), \quad \kappa = \left[\mathcal{L}(2) - (\mathcal{L}(1))^2 / \mathcal{L}(0) \right] / T \quad (2)$$

$$L_N = \kappa / (T\sigma). \quad (3)$$

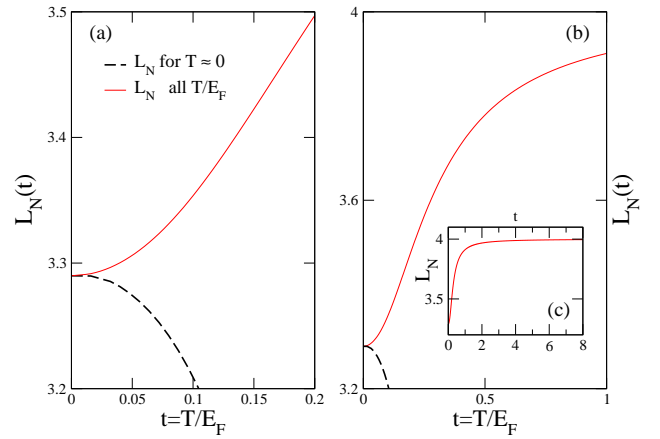


FIG. 1. (Color online) (a) The universal Lorentz number $L_N(t)$ Eq. 8, fitted to Eq. 11 is displayed by the continuous red line for $t > 0.2$. The $T \sim 0$ approximation, Eq. 12 is shown as a dashed black line. (b) The same as the left panel, now for $t \leq 1$. The inset (c) shows $L_N(t)$ from the quantum limit $\pi^2/3$ to the classical (Landau-Spitzer) limit of 4.

In SM we develop the reduced form

$$\mathcal{L}^{(\alpha)} = \left\langle \frac{1}{3} (\epsilon - \mu)^\alpha \tau_{ie}(\epsilon) (2\epsilon)^{3/2} \right\rangle. \quad (4)$$

The mean value $\langle \dots \rangle$ is defined by:

$$\langle g(\epsilon) \rangle = - \int_0^\infty d\epsilon \frac{f(\epsilon)}{d\epsilon} g(\epsilon) \quad (5)$$

$$f(\epsilon) = 1 / [1 + \exp(\epsilon - \mu) / T]. \quad (6)$$

The relaxation time τ_{ei} can be evaluated via the NPA using the static ion-ion structure-factor $S(k)$ and the cross section $\Sigma(\vec{k}, \vec{q})$. The latter is for the scattering of an electron of momentum \vec{k} with a momentum transfer \vec{q} [35]. In elastic collisions (with the internal structure of the ion held invariant), a weak pseudopotential can be constructed to describe the scattering [3]. The energy dependent $\tau_{ie}(\epsilon)$ can be written as

$$\tau_{ie}(\epsilon) = C_\tau \epsilon^{3/2} / C_{lg}. \quad (7)$$

Here the numerical coefficient C_τ and the Coulomb logarithm C_{lg} can be matched, as desired, to a sophisticated calculation of τ_{ie} or to a simple Landau-Spitzer form. Then it is shown in SM [33] that the $L_N(t)$ is given by:

$$L_N(t) = \frac{5I_4(\eta)}{3I_2(\eta)} - \left[\frac{4I_3(\eta)}{3I_2(\eta)} \right]^2, \quad t > 0 \quad (8)$$

$$= \pi^2/3, \quad t \sim 0 \quad (9)$$

$$I_n(\eta) = \int \frac{dx x^n}{1 + \exp(x - \eta)}, \quad \eta = \mu/T. \quad (10)$$

These results can be fitted to the formula

$$L_N(t) = \frac{a_0 + a_1 t + a_2 t^2 + a_3 t^3 + 4t^4}{1 + b_2 t^2 + t^4}. \quad (11)$$

The fit coefficients a_0, a_1, a_2, a_3 are $\pi^2/3, -0.0666174, 43.7111, 0.00994066$ respectively, while $b_2 = 11.010134$. This result does not include effects of ion-embedding in the electron fluid, or XC-effects. For high-density electron systems like aluminum or carbon at the densities studied here, ion-embedding effects mainly result in a rigid lowering of the continuum. When electron XC-effects are included, a_0 is modified from 3.29 to 3.328 near $T = 0$ for Al at 2.7 g/cm^3 , and to 3.194 for carbon at 10 g/cm^3 , but these are countered by other contributions. These many-body effects will be considered in a separate study.

The $t \simeq 0$ limiting form is obtained from the following.

$$\kappa = (1/3)C_e \langle V^2 \rangle \tau_{ie}, \quad t \sim 0 \quad (12)$$

Here C_e is the electron specific heat per particle, while $\langle V^2 \rangle$ is an electron mean square-velocity evaluated within the scattering region $E_F \pm T$ in k -space enclosing the Fermi energy. We compare this limiting form for $L_N(t \sim 0)$ with the fit form, Eq. 11, numerical equivalent to the analytic form, Eq. 8 in Fig. 1. The same curve $L_N(t)$ is obtained for all r_s, T given as a universal function of $T = T/E_F$. This universality is lost when XC-effects, embedding effects [36] are included. For instance, the modification of the specific heats can be calculated from the second derivative of the total electron free energy that includes finite- T XC-effects [21].

Thermopower and the Seebeck coefficient- The thermoelectric coefficient (Seebeck coefficient) $\theta(t)$ can be expressed as:

$$\theta(t) = -\frac{1}{eT} \frac{\mathcal{L}^{(1)}}{\mathcal{L}^{(0)}} = \left(\frac{4I_3}{3I_2} - \eta \right), \quad t > 0. \quad (13)$$

The above equation is not applicable at $T \simeq 0$. In the classical limit Eq. 13 takes the value $(4 - \eta)$.

Thermal conductivities of Al and carbon- Recoules et al [23] have calculated the electrical conductivity σ using QMD-KG and the corresponding κ via the kinetic coefficients for isochoric l -Al at the density 2.35 g/cm^3 from 1000K (0.0862 eV) to 10,000K (0.862 eV). Their results, as well as our results for σ evaluated from the pseudopotential, and the corresponding κ are shown in Fig. 2.

Direct experimental results for κ for liquid metals do not seem to be available. Leitner et al. [34] have reported accurate experimental isobaric electrical conductivities for l -Al near the melting point and *evaluated* κ using the ideal Lorentz number which is practically identical to the estimate from our Eq. 11 as well. Their isobaric density measurement is constrained to upper and lower estimates $\rho_1(T)$ and $\rho_2(T)$. We calculate σ, κ for the upper and lower sets of densities and compare them (see Fig. 3) with the results of Leitner et al [34]. Our theoretical analysis supports their lower density estimate ρ_2 .

High-temperature results- While experimental σ data are available near the melting point of common metals,

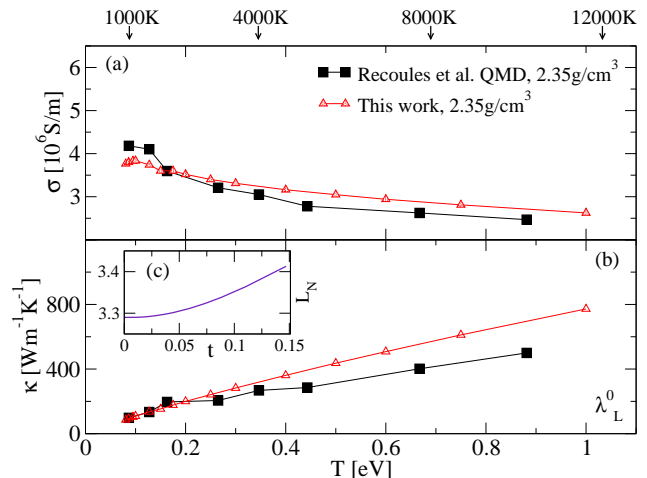


FIG. 2. (Color online) (a) The electrical conductivity σ_z for l -Al at 2.35 g/cm^3 from the NPA-pseudopotentials and the Ziman formula. The QMD-KG results of Recoules et al [23] are at 2.35 g/cm^3 . Panel (b) shows the corresponding κ . The inset (c) shows $L_N(t), t = T/E_F$ Eq. 11 used in calculating κ .

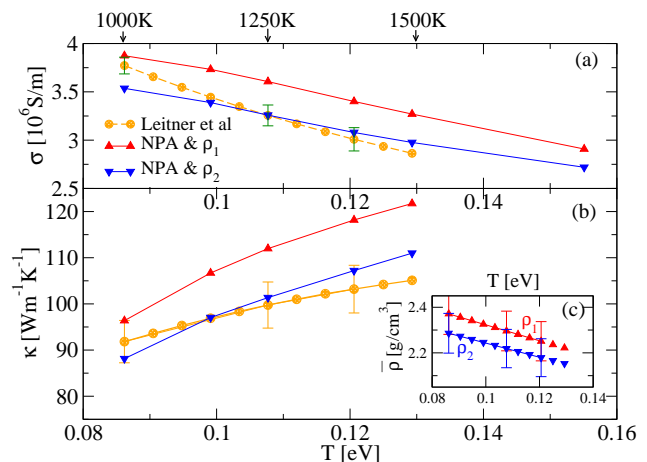


FIG. 3. (Color online) (a) The electrical conductivity σ_z for l -Al at isobaric densities ρ_1, ρ_2 from the NPA-pseudopotentials and the Ziman formula, compared with the experimental results of Leitner et al [34]. Panel (b) shows the corresponding κ calculated using the L_N of our theory, as well as the estimates in Ref. [34]. The inset (c) shows the two sets of densities ρ_1, ρ_2 that are upper and lower bounds to the actual isobaric density $\rho(T)$. The better estimate of $\rho(T)$ is possibly ρ_2 .

data at higher- T data are unavailable. Hence we compare our results with other theoretical results. While the σ_z calculated from a pseudopotential is for robust ions of charge \bar{Z} where the scattering electron does not interact with the weakly-bound electronic structure of the ion, the T-matrix approach [37] includes such interactions, as discussed further in SM [33]. Different approaches differ in the manner they deal with such ‘hopping electrons’ associated with clusters of ions [38] or an individual average ion, and in how they handle strong-scattering ef-

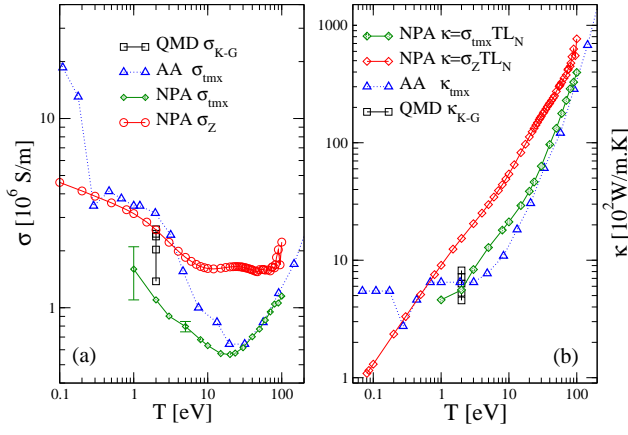


FIG. 4. (Color online) (a) The isochoric conductivities σ_z, σ_{tmx} calculated via the Ziman formula with NPA inputs, for l -aluminum, compared with selected AA and all QMD results as reported in Ref. [2]. (b) The NPA- κ obtained via Eq.11, as well as selected thermal conductivities κ reported in Ref. [2].

fects. Hence the σ calculated by the Ziman formula using a pseudopotential based on \bar{Z} , denoted here by σ_z , from a T-matrix, viz σ_{tmx} or from the K-G approach may differ for ions with loose internal structure and in the treatment of strong-scattering.

Given a σ , it appears that a good approximation to the corresponding κ can be obtained via the finite- T Lorentz number, viz., Eqs. 8,11. In the following and (in SM, for carbon at 3.6 g/cm^3), we present results for isochoric σ_z, κ for l -aluminum at 2.7 g/cm^3 and for l -carbon at 10 g/cm^3 , in Figs. 4, 5 respectively.

Discussion- The Lorentz number and the Hall coefficient are two quantities that are relatively independent of the details of the material and the microscopic interactions included in σ and κ . Thus, even a minimal model of the interactions may be expected to provide a good evaluation of L_N . This is already seen in the quantum and classical limits of L_N which are $\pi^2/3$ and 4 respectively.

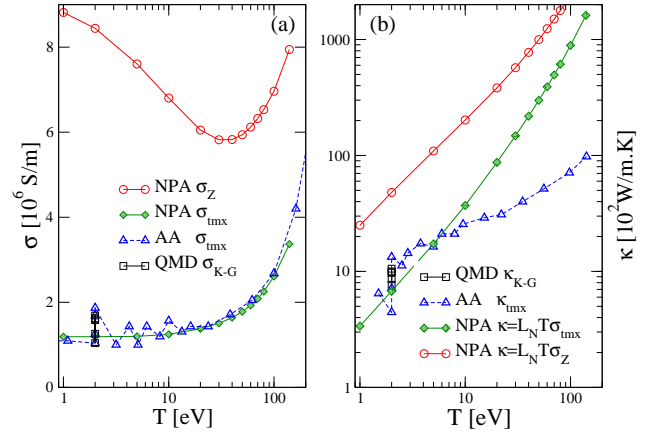


FIG. 5. (Color online) Results for l -carbon as in Fig. 4.

We show in SM that even at intermediate degeneracies, most of the complexities in $\mathcal{L}^{(\alpha)}$ factors cancel out in evaluating L_N . Hence our simplified evaluation of L_N is likely to have a larger regime of validity than expected.

The good agreement of the Ziman conductivity σ_z based on a pseudopotential, in the low- T regime as seen in Figs. 2, 3 shows that the assumption of weak scattering from an Al^{3+} ion with a rigid core is valid up to $T \sim 1 \text{ eV}$ for Al. As T increases, \bar{Z} begins to exceed 3 and acquires fractional values, e.g., 3.25 etc. Then hopping-electron distributions emerge and the calculated σ depends on how partially localized charges are dealt with in different conductivity models [25, 36, 39–46]. However, the σ_z model provides a rigorous estimate of the *elastic scattering* contribution from ions whose internal structures remain rigid. If the phase shifts from the NPA are used in a T-matrix calculation, denoted here as σ_{tmx} [33, 35], the corresponding lower conductivity of Al approaches that of other T-matrix models, both for σ and κ , with the latter evaluated here using our finite- T Lorentz number. For $T > E_F$, the NPA becomes increasingly like an AA model in that the free-electron density increment $\Delta n_f(r)$ is contained within the Wigner-Seitz ion sphere. Hence the good agreement in σ_{tmx} between the NPA and AA results for $T > E_F$ found for l -Al is not surprising. The agreement between κ values shows that the L_N used here for evaluating the NPA- κ is trustworthy. For l -carbon at 10 g/cm^3 , $E_F \simeq 60 \text{ eV}$. Hence the agreement in σ_{tmx} between NPA and AA even in the $t < 1$ range is interesting, but the AA-estimates of κ for $T > 10 \text{ eV}$ and from our calculations disagree, unexpectedly. Further result using the NPA and $L_N(t)$ equation are given in the supplemental material [33].

- [1] A. L. Kritchner, D. C. Swift, T. Döppner, B. Bachman, et al., Nature **584**, 51 (2020).
- [2] L. J. Stanek, A. KonoNov, S. B. Hansen, et al. *Review of the Second Charged-Particle Transport Coefficient Code-Comparison Workshop*. Unpublished (2023).
- [3] M. W. C. Dharma-wardana, Lucas J. Stanek, and

- Michael S. Murillo Phys. Rev. E **106**, 065208 (2022).
- [4] M. W. C. Dharma-wardana and F. Perrot, Phys. Rev. A **26**, 2096 (1982).
- [5] J.A. Gaffney, Suxing Hu, P. Arnault..E. Zurek et al. High Energy Density Physics, **28**, 7-24 (2018). <https://doi.org/10.1016/j.hedp.2018.08.00>

- [6] P. E. Grabowski, S. B. Hansen, M.S. Murillo, et al., High Energy Density Physics, **37**, 100905 (2020).
- [7] M. W. C. Dharma-wardana, Proceedings of the Conference in Density Functional Theory, Debrecen, 2015. Edited by K. Schwarz and A. Nagy. *Computation* **4** (2), 16 (2016).
- [8] M. W. C. Dharma-wardana, *SCCS-1977. Contrib. Plasma Phys.* **55**, No.2-3, 79-81 (2015).
- [9] A. Ng, *Int. J. Quantum Chem.* **112**, 150 (2012).
- [10] Niedermayer, M. Volkov, S. A. Sato, N. Hartmann, et al., *Phys. Rev. X* **12**, 021045 (2022).
- [11] Dongdong Kang, Kai Luo, Keith Runge, S. B. Trickey. *Matter and Radiation at Extremes*, **5**, 064403 (2020).
- [12] M. W. C. Dharma-wardana, *Physical Review Letters* **66**, 197 (1991).
- [13] M. W. C. Dharma-wardana, and François Perrot, *Phys. Rev. E* **58**, 3705 (1998).
- [14] M. W. C. Dharma-wardana, D. Neilson and F. M. Peeters *Phys. Rev. B* **99**, 035303 (2019).
- [15] Stanton, L. G., J. N. Glosli, and M. S. Murillo. *Physical Review X* **8**, 021044 (2018).
- [16] F. Perrot and M. W. C. Dharma-wardana, *Phys. Rev. A* **30**, 2619 (1984).
- [17] F. Perrot and M. W. C. Dharma-wardana, *Phys. Rev. B* **62**, 16536 (2000); *Erratum:* **67**, 79901 (2003); arXiv-1602.04734.
- [18] V. V. Karasiev, T. Sjostrom, J. W. Dufty, and S. B. Trickey, *Phys. Rev. Lett.* **112**, 076403 (2014)
- [19] S. Groth, T. Dornheim, T. Sjostrom, F.D. Malone, W. Foulkes, M. Bonitz, *Phys. Rev. Lett.* **119**, 135001 (2017). <http://dx.doi.org/10.1103/PhysRevLett.119.135001>.
- [20] Tobias Dornheim, Simon Groth, Michael Bonitz *Physics Reports* **744**, 1-86 (2018), <https://doi.org/10.1016/j.physrep.2018.04.001>.
- [21] V. Karasiev, S. B. Trickey and J. W. Dufty. *Phys. Rev. B* **99**, 195134 (2019)
- [22] M. P. Desjarlais, J. D. Kress, and L. A. Collins, *Phys. Rev. E* **66**, 025401 (2002).
- [23] V. Recoules and J. P. Crocombette, *Phys. Rev. B* **72**, 104202 (2005).
- [24] S. L. Adler, *Phys. Rev.* **126**, 413 (1962)
- [25] W. Johnson, *High Energy Density Physics* **5**, 61-67 (2009).
- [26] M. Kuchiev and W. Johnson, *Phys. Rev. E.* **78**, 026401 (2008).
- [27] N. W. Ashcroft and N. D. Mermin, *Solid State Physics*, Ch. 13. Saunders College, Philadelphia, USA (1976).
- [28] L. Spitzer and R. Härm, *Phys. Rev.* **89**, 977 (1953).
- [29] P. S. Shtermin and D. G. Yakovlev, *Phys. Rev. D* **74**,043004 (2006).
- [30] H. Reinholz, G. Röpke, S. Rosmej, and R. Redmer, *Phys. Rev. E* **91**, 043105 (2015).
- [31] M. P. Desjarlais, C. R. Scullard, L. X. Benedict, H. D. Whitely, R. Redmer, *Phys. Rev. E* **95**, 033203 (2017).
- [32] C. F. Richardson and N. W. Ashcroft, *Phys. Rev. B* **50**, 8170 (1994).
- [33] Supplementary material. This covers (i) Derivation of the finite- T form of the Lorentz number $L_n(t)$. (ii) Electron-electron interactions in DFT and in conventional approaches. (iii) The electrical conductivity from Pseudopotentials and from the T-matrix form of the scattering cross section. (iv) Results for l -Al at 2.7 g/cm^3 , l -carbon at 10 g/cm^3 , and at the “diamond-like” density of 3.6 g/cm^3 .
- [34] M. Leitner, T. Leitner, A. Schmon, K. Aziz and G. Pottlacher *Metallurgical and materials transactions A.* **48 A**, 3036 (2017).
- [35] F. Perrot and M. W. C. Dharma-wardana, *Int. J. of Thermophys* **20**, 1299 (1999).
- [36] F. Perrot and M.W.C. Dharma-wardana, *Phys. Rev. E.* **52**, 5352 (1995).
- [37] R. Evans, B.L. Gyorffy, N. Szabo, and J.M. Ziman, in *The Properties of Liquid Metals*, edited by S. Takeuchi (Wiley, New York, 1973).
- [38] M.W.C. Dharma-wardana and F. Perrot, *Phys. Rev. A* **45**, 5883 (1992).
- [39] P.A. Stern, S.B. Hansen, B.G. Wilson, W.A. Isaacs, *High Energy Density Phys.* **3**, 278 (2007).
- [40] M. S. Murillo, J. Weisheit, S. B. Hansen, and M. W. C. Dharma-wardana, *Phys. Rev. E* **87**, 063113 (2013).
- [41] Y. T. Lee and R. M. More, *Phys. Fluids* **27**, 1273 (1984).
- [42] F. Perrot, M.W.C. Dharma-wardana, *Phys. Rev. A* **36**, 238–246 (1987).
- [43] Balas F. Rosznyi, *High Energy Density Physics* **4**, 64-72 (2008).
- [44] V. D. Filinov, P. R. Levashov, A. V. Botan, Michael Bonitz, and V. Fortov, *J. Phys. A: Mathematical and Theoretical.* **42**, 214002 (2009).
- [45] C. E. Starrett, D. Saumon, J. Daligault, and S. Hamel, *Phys. Rev. E* **90**, 033110 (2014).
- [46] Nadine Wette and J-C Pain, *Phys. Rev. E* **108**, 015205 (2023)